Segmented Polyurethane Nanocomposites: Impact of Controlled Particle Size Nanofillers on the Morphological Response to Uniaxial Deformation

Bradley Finnigan,[†] Kevin Jack,[‡] Kayleen Campbell,[†] Peter Halley,[†] Rowan Truss,[†] Phil Casey,[§] David Cookson,[⊥] Stephen King,[#] and Darren Martin*,[†]

School of Engineering and the Centre for Nanotechnology and Biomaterials, The University of Queensland, Brisbane, Queensland 4072, Australia; CSIRO Manufacturing and Infrastructure Technology, Private Bag 33, Clayton South, VIC 3169, Australia; Australian Synchrotron Research Program, Bldg. 434, 9700 South Cass Ave, Argonne, Illinois 60439; and ISIS Facility, Rutherford Appleton Laboratory, Chilton, Didcot, Oxfordshire OX11 0QX, U.K.

Received April 26, 2005; Revised Manuscript Received June 2, 2005

ABSTRACT: A series of TPU nanocomposites were prepared by incorporating organically modified layered silicates with controlled particle size. To our knowledge, this is the first study into the effects of layered silicate diameter in polymer nanocomposites utilizing the same mineral for each size fraction. The tensile properties of these materials were found to be highly dependent upon the size of the layered silicates. A decrease in disk diameter was associated with a sharp upturn in the stress−strain curve and a pronounced increase in tensile strength. Results from SAXS/SANS experiments showed that the layered silicates did not affect the bulk TPU microphase structure and the morphological response of the host TPU to deformation or promote/hinder strain-induced soft segment crystallization. The improved tensile properties of the nanocomposites containing the smaller nanofillers resulted from the layered silicates aligning in the direction of strain and interacting with the TPU sequences via secondary bonding. This phenomenon contributes predominantly above 400% strain once the microdomain architecture has largely been disassembled. Large tactoids that are unable to align in the strain direction lead to concentrated tensile stresses between the polymer and filler, instead of desirable shear stresses, resulting in void formation and reduced tensile properties. In severe cases, such as that observed for the composite containing the largest silicate, these voids manifest visually as stress whitening.

Introduction

Thermoplastic polyurethanes (TPUs) are linear, segmented copolymers consisting of alternating hard and soft segments. The hard segment is composed of alternating diisocyanate and short chain extender molecules (i.e., diol or diamine), while the soft segment is formed from a linear, long-chain diol. Phase separation occurs in TPUs because of the thermodynamic incompatibility of the hard and soft segments. The segments aggregate into microdomains resulting in a structure consisting of glassy or semicrystalline hard domains and rubbery soft domains that are below and above their glass transition temperatures at room temperature, respectively.

The morphology of TPUs as well as its relationship to the thermal and mechanical properties has long been a topic of interest.[1−5] It is often difficult to visualize the morphology via transmission electron microscopy (TEM) because of the low electron density contrast between the soft and hard segments and the imperfect phase separation that generally occurs. Nonetheless, globular, cylindrical, and lamellar morphologies have been evidenced via TEM depending on the composition of the TPU and the processing route.[6−11] Atomic force microscopy (AFM) is proving to be a more effective and time-efficient technique for resolving the phase morphology of TPUs on the nanoscale. In recent years globular, cylindrical, and lamellar-like morphologies have been reported with this technique.[12−15]

Small-angle X-ray scattering (SAXS) is one of the most powerful techniques for studying the phase morphology of TPUs.[16,17] The use of synchrotron radiation as the X-ray source has permitted morphological changes to be followed in real time. Significant advancements in the understanding of TPU morphology and its complex thermal behavior have come through the use of DSC in combination with SAXS,[3] wide-angle X-ray scattering (WAXS),[4] and Fourier transform infrared (FTIR) spectroscopy.[18] High-intensity SAXS has been used to follow the phase separation kinetics during cooling from the melt state[19,20] and polymerization[21] and combined with FTIR to simultaneously follow the phase separation and reaction kinetics during polymerization.[22] The use of SAXS,[5,23−28] WAXS,[1,25,29] and FTIR dichroism[5,25,30−35] during uniaxial extension and cyclic loading has also enabled the microstructural changes responsible for the observed macroscale stress−strain behavior to be better understood. Generally speaking, initial deformation takes place in the soft phase because of its lower modulus, and the long axis of the hard domains orient parallel to the direction of strain. As the soft segments are stretched further apart, stress is transferred to the hard domains, causing them to rotate such that the segments within the domains are aligned parallel to the strain direction. As the strain increases further, the hard domains begin to fragment into

[†] School of Engineering, The University of Queensland.
[‡] Centre for Nanotechnology and Biomaterials, The University of Queensland.
[§] CSIRO Manufacturing and Infrastructure Technology.
[⊥] Australian Synchrotron Research Program.
[#] Rutherford Appleton Laboratory.
* To whom correspondence should be addressed. E-mail: darrenm@cheque.uq.edu.au.

10.1021/ma0508911 CCC: $30.25
Published on Web 07/26/2005

smaller structures, and the hard segments are pulled out of the domains. The aligned soft and hard segments form a fibrillar structure that may be accompanied by soft segment crystallization. Note that the exact deformation mechanism depends on the structural integrity and shape of the domains.[23,24]

In recent times nanometer-sized layered silicates have been introduced into many host polymers.[36−38] This interest was initiated by the large improvements in stiffness and heat distortion temperature Kojima et al. achieved by incorporating layered silicates into nylon-6 at very low loadings (compared to traditional fillers).[39] The majority of nanocomposite papers have focused on how the silicate surface treatment and concentration affect various properties of these materials. It was therefore of interest to investigate the effect of the silicate platelet size or disk diameter on the properties of a TPU. Of the small number of investigations into the effect of silicate size on nanocomposite structure and performance, all have used different clay minerals to obtain the different size fractions.[40−45] However, changing the mineral phase complicates the interpretation of results because the different minerals have their own unique properties. For example, if the cation exchange capacity (CEC) differs between clay minerals or deposits, then the concentration and conformation of a surfactant ion-exchanged to the silicates will be different. The result will be a different polymer−filler interaction that leads to altered polymer intercalation, organosilicate dispersion, and, of course, material properties.

This particular problem of surfactant coverage can be overcome to a certain extent, at least for alkylammonium-modified silicates, if the same surfactant chain density can be achieved for each silicate under investigation.[46−49] Krishnamoorti et al.[40−42] used this concept to study the influence of platelet size on the phase-separated morphologies of block copolymers[41,42] and polymer blends.[40] In these studies Laponite (30 nm, CEC = 0.75 mequiv/g) and montmorillonite (500 nm, CEC = 0.9 mequiv/g), modified with dimethyldioctadecylammonium, and fluorohectorite (10 μm, CEC = 1.5 mequiv/g), modified with trimethyloctadecylammonium, were utilized to obtain the different size fractions with similar organic coverage. These studies revealed that the microphase morphologies of the block copolymers and polymer blends were dependent upon the platelet size.

Aside from the evidence that layered silicates can significantly change the microphase domain size and shape of block polymers,[50] which in turn leads to altered properties (and a potential route to control morphology on the nanoscale), one would expect the size of the silicate particles to play an important role in material properties in its own right. Wang et al. studied the effect of silicate diameter on the solid state[45] and melt state[44] properties of maleated-polyethylene (ma-PE) nanocomposites and found that the composite containing 100 nm disks displayed superior properties and processability over the neat ma-PE and 25 nm disk composites. Molecular dynamics simulations by Gersappe suggest that the smaller, and therefore more mobile fillers, would offer larger improvements in toughness than their larger counterparts, particularly in rubbery host polymers.[51]

In this work four size fractions of Somasif MEE (organically treated, synthetic fluoromica, CO-OP Chemical Co.) have been incorporated into a TPU. To the best of our knowledge, this is the first time the effect of disk diameter has been studied using the same layered silicate. The tensile behavior of the nanocomposite containing the smallest filler is exceptional, and as a result, this paper will focus primarily on the microstructure of this series of materials and their response to tensile deformation as studied by SAXS. Furthermore, we provide a model for the means of describing how the size of the filler particle affects both the microstructure and mechanical properties in these materials.

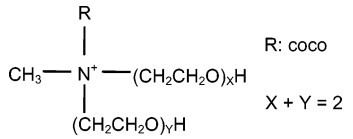

Figure 1. Chemical structure of Somasif MEE surfactant.

Experimental Section

Materials. The TPU employed in this study consisted of a 1000 g/mol poly(tetramethylene oxide) (PTMO) soft segment with a 4,4′-methylene diphenyl diisocyanate (MDI) and 1,4-butanediol (BDO) hard segment. The hard segment concentration was 35 wt %, resulting in a soft elastomer of Shore Hardness 80A. The TPU was supplied by Urethane Compounds, Melbourne. The number-average molecular weights (M_n) and polydispersity indices (PDI) of the host polymer was determined to be 216 000 and 1.8, respectively, by gel permeation chromatography. The hard segments are glassy, and the glass transition temperature and microphase separation transition of the TPU were determined via differential scanning calorimetry to be −52 and 130 °C, respectively.[52]

Somasif MEE (MEE) was supplied by CO-OP Chemical Co. (Japan). MEE is a synthetic fluoromica with the chemical composition of $Na_{0.66}Mg_{2.68}(Si_{3.98}Al_{0.02})O_{10.02}F_{1.96}$ and CEC of 115 mequiv/g.[53] The MEE variant of Somasif has a dipolyoxyethylenecocomethylammonium surface modification (Figure 1).

Sample Preparation. Different size fractions of MEE (30, 75, 200, and 650 nm) were obtained via a proprietary, high-energy milling process. The preparation and characterization of these silicates have been discussed elsewhere.[54] Nanocomposite films were prepared via solvent casting. A 5 wt % solution of dried MEE in toluene was ultrasonicated for 2 min before being added to a 5 wt % solution of TPU in dimethylacetamide (DMAc). The combined solution was then mixed vigorously for 1 min in a high-shear homogenizer, followed by stirring for 24 h at room temperature with a magnetic stirrer. The mixture was then cast onto glass plates, and the films were dried under a nitrogen atmosphere at 50 °C for 48 h and subsequently dried under vacuum at 50 °C for 12 h. The films were then annealed under vacuum at 80 °C for 12 h and stored under ambient conditions for 1 month prior to characterization. The nanocomposites contained 3 wt % of organosilicate, and the film thickness was 0.5 mm.

Characterization. TEM samples were cut on a Leica Ultracut S ultramicrotome with a glass knife at −100 °C and collected on 400 mesh copper grids. Images were obtained using a JEOL JEM 1010 TEM operated at 100 keV. The size of the layered silicates were estimated by recording the lengths of a large number of platelets and particles in a number of TEM images to obtain a size distribution.[55]

X-ray diffraction (XRD) analysis was carried out on a Bruker D8 Advance X-ray diffractometer using Cu Kα radiation generated at 40 kV and 30 mA. Samples were scanned at 2.4°/min in the range of $2\theta = 1°-40°$ using a step size of 0.02°. The MEE powders were lightly pressed and flattened to obtain a smooth surface prior to testing.

Tensile tests were carried out at 25 °C on an Instron model 4505 universal testing machine using five replicates of each material. Dumbbells were punched from the films using an ATSM D-638-M-3 die and strained at 50 mm/min. Young's

modulus was estimated from the slope at 0% strain on the tensile curve.

Scattering Measurements. Small-angle neutron scattering (SANS) experiments were performed on the LOQ station at the ISIS pulsed neutron source, Rutherford Appleton Laboratory, UK. The TPU had sufficient neutron density contrast between the hard and soft phase such that deuteration was not required. A sample thickness of 1 mm and a beam size of 8 mm diameter were used. 2D-SANS data were collected over the course of 30 min for each sample. All neutron scattering data were corrected for sample transmission, thickness, and background scattering. The data were converted to absolute units by calibrating with a blend of deuterated and hydrogenated polystyrenes of known absolute cross section.[56]

In-situ tensile deformation studies using SAXS were performed on station 15-ID-D (ChemMatCARS) of the Advanced Photon Source at Argonne National Laboratory, Argonne, IL. Three X-ray wavelength/camera length setups were used to capture the q ranges of interest: 1.54 Å/6.817 m (long), 1.05 Å/1.91 m (medium), and 0.41 Å/0.563 m (short). The beam size at the sample position was ~0.3 mm in the strain direction and 0.2 mm in the transverse direction. Data acquisition times of 1, 10, and 5 s were required for each measurement at the long, medium, and short camera lengths, respectively. The data were normalized against the intensity measured at the beamstop to account for changes in transmission due to changes in sample thickness with strain and further corrected for background scattering. The SAXS and SANS data were both corrected for thermal density fluctuations using the procedure of Bonart.[57]

SAXS samples were cut with a nonstandard dumbbell die with a narrowest width of 5 mm. The nonstandard dumbbell resulted in higher strain at break values in the SAXS experiments compared with those measured on the Instron machine using the ATSM D-638-M-3 die. A purpose-built tensometer was constructed for the SAXS experiments. The design features include a travel of 400 mm to allow the complete tensile curve to be studied, dual tensile actuation in order to maintain the sample's center in the beam, and self-tightening grips that prevent slippage. Specimens were strained at a rate of 15 mm/min.

Scattering Analysis. Laity et al.[58] assessed the ability of a number of scattering models based on different morphologies to reproduce the scattering features observed for PTMO/MDI/BDO-based TPUs with various compositions. Spherical models based on a Zernike−Prins type lattice or a Percus−Yevick liquid type structure were found to most accurately fit the data. The Zernike−Prins model was used by Laity et al. to successfully fit SAXS data from TPUs subjected to uniaxial deformation.[26] The Zernike−Prins model was chosen over the Percus−Yevick model for the uniaxial deformation study because it directly provides an estimate of the interdomain distance. Visser and Cooper[59] and Krakovsky et al.[60] have also used the Percus−Yevick model to fit the scattering peak and high-q tail of polyurethane ionomers and cross-linked polyurethanes, respectively. While both of these models have been found to be consistent with the data presented here, only the Zernike−Prins modeling will be discussed.

The scattering from two phase systems can be represented as the product of the form factor, $P(q)$, and the structure factor, $S(q)$

$$I(q) = AP(q)\,S(q) \tag{1}$$

where q is the scattering vector and A consists of both instrument and sample dependent terms and can be treated as a scaling factor. $P(q)$ is a function that describes the interference effects between X-rays scattered by different parts of the same scattering body (microdomain) and is dependent upon both the size and shape of the scattering body.[61] $S(q)$ is a function that describes the interference effects between X-rays scattered by different scattering bodies in the sample and depends on their relative positions.[61]

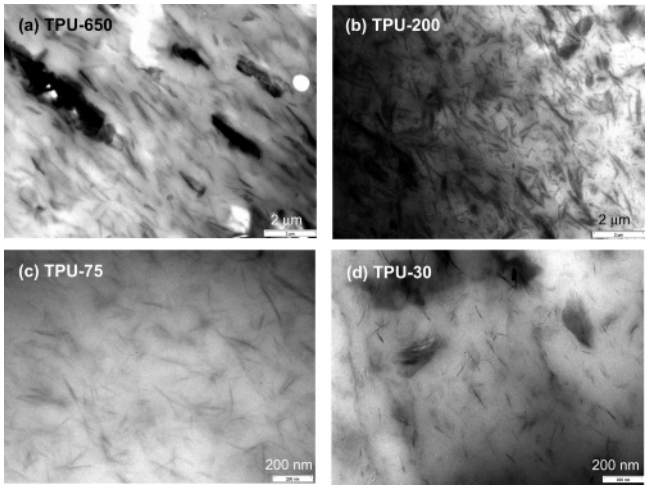

Figure 2. TEM images of TPU containing 3 wt % of (a) MEE-650, (b) MEE-200, (c) MEE-75, and (d) MEE-30.

The form factor of a sphere of radius (R) is given by

$$P(q) = \left\{3\,\frac{\sin(qR) - qR\,\cos(qR)}{(qR)^3}\right\}^2 \tag{2}$$

Zernike−Prins Model. The Zernike−Prins model[58] assumes that the positions of the scattering bodies in a medium can be described in any direction by a distorted one-dimensional statistical lattice

$$S(q) = \frac{1 - A^2}{1 - 2A\,\cos(qd) + A^2} \tag{3}$$

where

$$A = \exp\left\{-\frac{q^2\sigma^2}{2}\right\} \tag{4}$$

for the case of a Gaussian distribution of nearest-neighbor distances (d) on the lattice, with standard deviation σ.

Hermans Orientation Parameter. The orientation of the platelets during tensile deformation was expected to be an important factor contributing to the tensile properties displayed by the nanocomposites.[62−64] The Hermans orientation parameter (f)[65,66] was used to assess the orientation of the different sized fillers during tensile deformation and is given by the following equation

$$f = \frac{3\langle\cos^2\Theta\rangle - 1}{2} \tag{5}$$

where

$$\langle\cos^2\Theta\rangle = \frac{\int_0^{\pi/2} I\,\cos^2\Theta\,\sin\Theta\,\mathrm{d}\Theta}{\int_0^{\pi/2} I\,\sin\Theta\,\mathrm{d}\Theta} \tag{6}$$

The value of f is equal to 1 or $-1/2$ when the orientation of the system is completely aligned along $\pi/2$ or 0 directions, respectively, and $f = 0$ when the system is completely random.

Results

Silicate Size and Nanocomposite Structure. TEM images of the nanocomposites containing the four size fractions of MEE are displayed in Figure 2. The mean effective diameter of the different size fractions was measured in the nanocomposites to be approximately 30, 75, 200, and 650 nm using the method described by Fornes and Paul.[55] The size statistics of the silicates are

Table 1. TEM Size Statistics

	diameter (nm)	interparticle distance (nm)	no. of particles counted
MEE-30	29 ± 17	27	564
MEE-75	75 ± 36	68	420
MEE-200	203 ± 191	122	374
MEE-650	644 ± 526	177	504

given in Table 1, and from this point onward the silicates and nanocomposites containing them will be referred to as MEE-*X* and TPU-*X*, respectively, where $X = 30$, 75, 200, and 650 (i.e., the mean effective diameter).

In general, the MEE silicates dispersed and delaminated well in the TPU because the hydroxyl functionality of the surfactant provided a favorable thermodynamic driving force for TPU intercalation.[46−48] TPU-650 exhibited an ordered intercalated structure that also contained larger silicate stacks or tactoids (on the order of several microns) interdispersed throughout the material. The degree of dispersion and delamination was observed to improve as the diameter decreased. This is attributed to a reduction in spatial restrictions, tactoid size of the milled MEE powders, and an increase in nanofiller mobility. To achieve complete exfoliation, the volume fraction of layered silicates must be less than 1/aspect ratio.[67] In this study, the composites incorporate 3 wt % of MEE, which equates to approximately 1 vol % inorganic material. This means that only MEE-30 was spatially capable of fully delaminating at a 3 wt % loading without experiencing frustrated orientational freedom. Note that MEE-650 and MEE-200 have interparticle distances that are significantly smaller than their size (Table 1). The large platelet stacks observed in the composite containing MEE-650 suggest that as the disk diameter increases, the nanofiller mobility decreases, making it more difficult for the intercalated polymer to peel the platelets away from the well-intercalated tactoids. The milling process most likely reduced the tactoid size of the milled silicate powders, further easing their delamination in the TPU.

XRD patterns of the organosilicates are shown in Figure 3a. The small peak at 1.93° is assigned to a superstructure composed of alternating high and low charge layers. The superstructure originates from Somasif's charge heterogeneity that causes different amounts of alkylammonium ions to intercalate the layers, and hence monlayer−bilayer or bilayer−pseudotrilayer arrangements to occur, depending on the size of the alkylammonium.[53,68] When regular interstratified structures form, the superstructure reflection is observed.[69,70] Because the superstructure reflection was not clearly observed in MEE−30 and MEE-75, this indicates that the ordering of the high and low charge layers may have become more random during milling. As the particle size reduced, the peaks became broader and the signal intensity decreased, which also made it more difficult to see the superstructure reflection. The d_{002} reflection at $2\theta = 3.97°$ for MEE-650, and at $2\theta = 4.2°$ for the milled silicates, is the sum of the scattering from the two layers and corresponds to an basal spacing of approximately 22 and 21 Å for the nonmilled and milled silicates, respectively. Thermogravimetric analysis and FTIR results have indicated that the chemical structure and concentration of the dipolyoxyethylenecocomethylammonium surfactant on the silicate surface did not change during the milling process.[54] Instead, the lower basal spacing of the milled silicates may be a result of altered surfactant conformations. The peak at 5.79° is the 003 interference of the superstructure (i.e., 5.79°/3 = 1.93°).

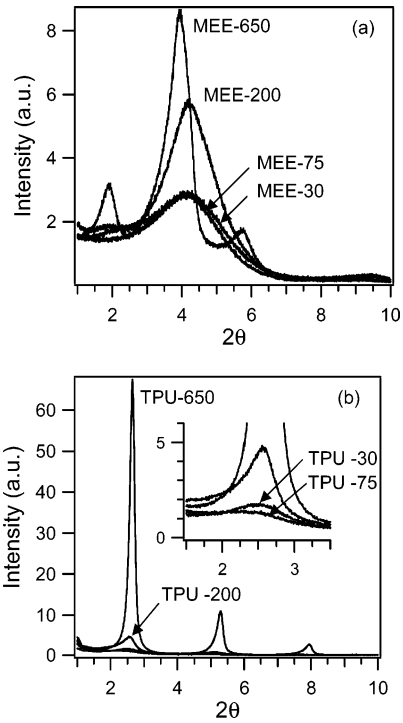

Figure 3. XRD patterns of (a) organosilicates and (b) TPU composites.

XRD patterns of the nanocomposites are shown in Figure 3b. The basal spacing for the nanocomposites was determined from the d_{001} peak at $2\theta = 2.6°$ to be 34 Å, which illustrates the good degree of polymer intercalation achieved in this system. The basal spacing is approximately the same in all of the composites, providing further evidence that the four size fractions of MEE are thermodynamically equivalent.[46−48] The decrease in intensity and peak broadening observed with decreasing diameter and stack size is due to a reduction in the length and ordering of the repetitive layer structure.

Tensile Properties. The initial part of the tensile curves of the nanocomposites is given in Figure 4a. As expected from composite theory, the modulus of the composite is observed to increase with platelet size. Increases in modulus result from the mismatch in the elastic constants of the filler and polymer. Polymer in the vicinity of the silicate becomes mechanically restrained, enabling a significant proportion of the load to be transferred to the silicate.[55,64] The amount of restrained polymer increases with diameter: resulting in an increase in modulus.

The complete tensile curves of the MEE composites are given in Figure 4b. The size of the silicates has a profound effect on the tensile properties. Most notably, there is a pronounced increase in the upturn of the stress−strain curve and an increase in tensile strength associated with decreasing platelet size. The tensile behavior of TPU-30 is exceptional and resembles more closely the mechanical characteristics of a highly drawn poly(urethane−urea) fiber (Lycra or Spandex). There are a number of possible explanations for this behavior. First, the small silicates may be able to act as nucleation sites, thereby enhancing soft segment crystallization. Second, physical interactions between the polymer and

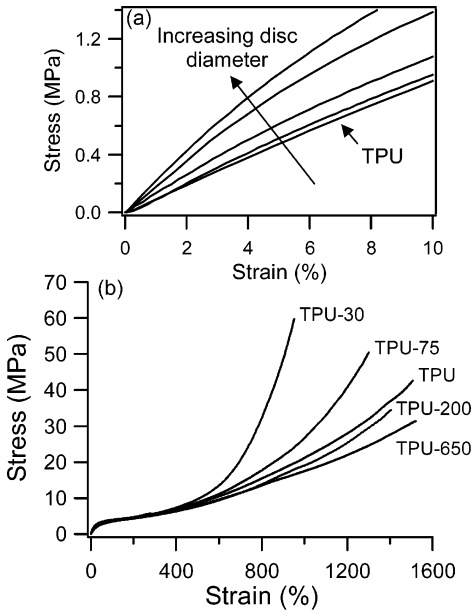

Figure 4. Effect of silicate size on the (a) modulus and (b) stress−strain curve.

the smaller, more mobile silicates may be strengthening the TPU by increasing secondary bonding and/or physical entanglements to reduce slippage during straining. Third, the silicates may be able to alter the static (or strained) microphase morphology of the TPU in such a way that results in improved tensile properties. Such an alteration to the microphase morphology may be critically dependent upon the size of the filler. As mentioned in the Introduction, the dependence of block copolymer domain size and shape on the platelet size has been reported.[41,42] SAXS experiments were therefore performed as a function of strain in an effort to better elucidate the mechanisms responsible for the observed tensile properties in these materials.

Silicate Orientation. 2D SAXS patterns obtained at the longest camera length are given for TPU-30 as an example at selected strains in Figure 5a. The initially isotropic SAXS pattern is observed to become anisotropic as the strain increases. The stripe formed along the meridian or transverse direction indicates significant platelet alignment in the direction of strain. The SAXS data collected at the longest camera length are believed to be almost entirely due to scattering from the silicates. This is demonstrated in Figure 5b where it can be seen that the intensity of the radially averaged 1D scattering profile from the pure TPU is negligible compared to that of the composites (TPU-200 shown as an example). The Hermans orientation parameter, f, was used to assess the orientation of the silicates during uniaxial deformation. An example of the azimuthally averaged data used to calculate f is shown in Figure 5c. f was calculated at $q = 0.003$ Å^{-1} and $q = 0.005$ Å^{-1} where scattering is dominated by the silicates (Figure 5b). The results obtained were the same for both q values, and it is believed that f is independent of q in this region. The orientation parameter is given as a function of strain in Figure 5d.

In the initial stages of deformation the largest silicate is observed to align the most in the direction of strain, followed by the smallest silicate, and finally the intermediate size fractions are the least aligned. As the specimens were strained further, the smallest silicate displayed the highest degree of alignment and the orientation of the intermediate size fractions became comparable to the largest size fraction. The orientation

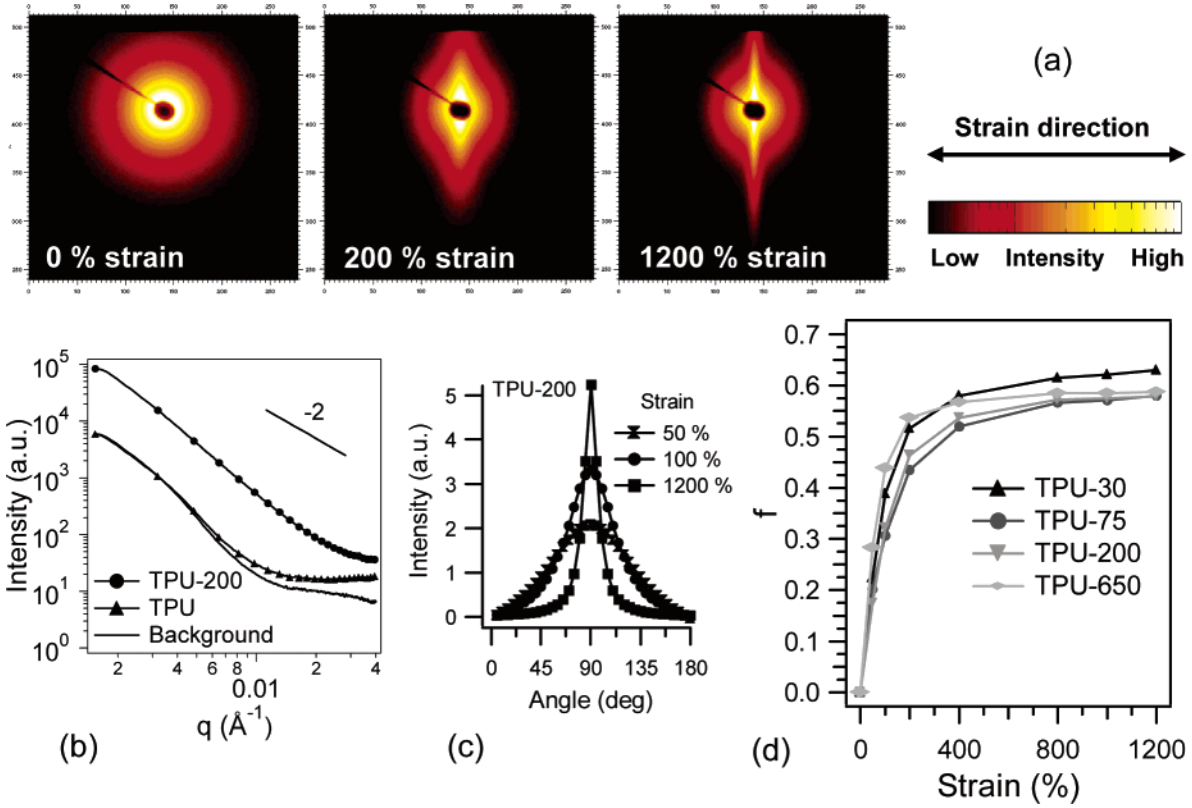

Figure 5. (a) 2D SAXS patterns at selected strains for TPU-30, (b) 1D SAXS profiles illustrating the dominant silicate scattering and power-law behavior, (c) azimuthal scan of scattered intensity at $q = 0.003$ Å^{-1} for TPU-200 at selected strains, and (d) Hermans orientation parameter as a function of strain.

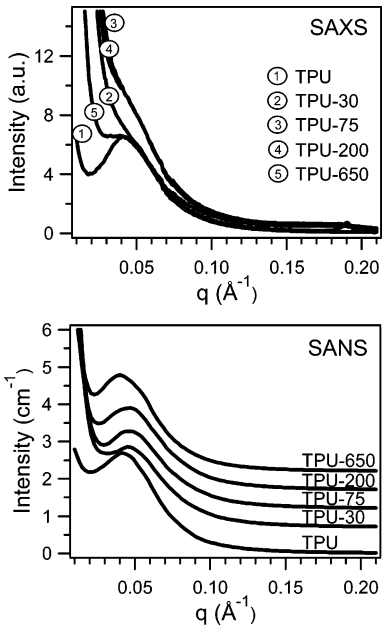

Figure 6. 1D SAXS and SANS profiles of undeformed samples.

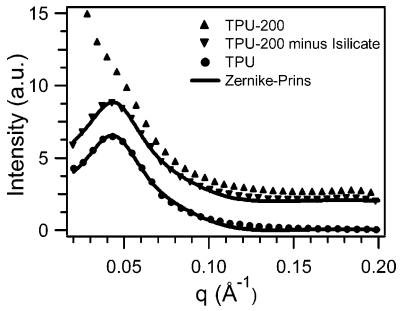

Figure 7. Example Zernike−Prins fits for TPU and TPU-200 following subtraction of silicate scattering. TPU-200 curves have been shifted vertically for clarity.

Table 2. Morphological Data Obtained from Zernike−Prins Fits of SANS Data

	Zernike−Prins model		
	d (nm)	R (nm)	σ/d
uncertainty[a]	± 0.5	± 0.5	± 0.05
TPU	8.5	3.5	0.66
TPU-30	10.4	3.1	0.49
TPU-75	10.2	3.1	0.50
TPU-200	8.4	3.2	0.63
TPU-650	9.5	3.4	0.63

[a] Expected uncertainty due to sample variations and curve fitting.

of the silicates is clearly not a simple function of size (silicate mobility), but depends also on other factors such as the initial state of dispersion and spatial restrictions encountered from neighboring platelets. The higher spatial restrictions experienced by the larger silicates are likely to have prevented them from orienting to the same extent as MEE-30 at high elongation.

TPU Microphase Morphology. SAXS data relating to the TPU microphase morphology were obtained at the medium camera length setup. The radially averaged 1D SAXS and SANS profiles of the undeformed materials are shown in Figure 6. The TPU shows an upturn in intensity at low q followed by a broad peak corresponding to the microphase periodicity in the material.[17] In the SANS nanocomposite profiles, the $P(q)$ scattering contribution from the silicates is only evident at low q as an increased upturn in the intensity, whereas this contribution is more significant in the SAXS nanocomposite profiles. This is because the neutron scattering length density of the silicates is comparable to that of the TPU hard segment, whereas the X-ray scattering length density of the silicate is much higher than that of the TPU. While SANS had an advantage for studying the static TPU morphology in the nanocomposites, the disadvantage of SANS in this study was that the data collection time was significantly longer. For this reason SANS was not used to study the morphological response to tensile deformation because substantial relaxation of the polymer would occur during the measurements.

Zernike−Prins (ZP) Analysis. To fit the SAXS nanocomposite profiles with the ZP model, it was necessary to estimate and subtract the silicate scattering. Layered silicates exhibit a power-law dependence at q less than the d_{001} or interlayer spacing, $I(q) = Aq^m$.[67] This dependence was determined for each of the composites from the data obtained at the longest camera length where the TPU scattering was negligible (see Figure 5b). The silicate scattering was then subtracted, and an example of this, along with the ZP fit to the data, is shown for TPU-200 in Figure 7. The approximation and subtraction of the silicate scattering are thought to be reasonable, and the ZP model was able to accurately reproduce the scattering peak and high q data. This model, however, was unable to reproduce the upturn in intensity at low q, consistent with previous findings.[59,60]

In addition, the model data contain a small minima centered at approximately $q = 0.13$ Å^{-1}, which is not present in the scattering data (Figure 7). This minima is due to the assumption of a monodisperse spherical form factor. The use of a polydisperse form factor smears out the minima; however, the solution to the model is more complex, and an additional fitting parameter is introduced that cannot be solved independently.[59,71] Polydisperse sphere modeling was attempted here, and while the minima was smeared out, no additional insight was gained.

The morphological data obtained from the ZP analysis of the SANS data are given in Table 2. In all materials, the interdomain spacing (d) and radius of the hard domains (R) were estimated to be approximately 10 and 3.3 nm, respectively. The SAXS results are consistent with this and are presented later in Table 3. The Percus−Yevick model, while not discussed in depth here, was equally able to fit the scattering data. An R value of 3.3 nm was also estimated by the Percus−Yevick model, and the hard domain volume fraction was estimated to be 0.23 out of a possible 0.3, indicating that approximately 77% of the hard segments are present in the hard domains. The volume fraction of hard segment participating in the hard domains reported here is significantly higher than that reported by Laity for compression-molded TPUs based on PTMO/MDI/BDO.[26]

Strained Morphology. 1D SAXS profiles for the pure TPU averaged over 10° sectors in the strain and transverse directions are given in Figure 8 along with ZP fits to the data. Previously, morphological changes had only been followed to 150% strain using the ZP model due to limitations of the straining apparatus.[26] Here the ZP model was applied at a number of intervals up to 300% strain as well as at two high strains, 800%

Table 3. Morphological Data Obtained from Zernike−Prins Fits of SAXS Data

		strain direction			transverse direction		
strain (%)		*d* (nm)	*R* (nm)	*σ*/*d*	*d* (nm)	*R* (nm)	*σ*/*d*
uncertainty[a]		± 0.5	± 0.5	± 0.05	± 0.5	± 0.5	± 0.05
0	TPU	9.9	3.4	0.56	10.1	3.5	0.55
	TPU-30	9.3	3.2	0.63	9.2	3.2	0.63
	TPU-75	9.5	3.3	0.55	9.6	3.3	0.56
	TPU-200	10.2	3.4	0.55	10.2	3.4	0.54
	TPU-650	10.2	3.3	0.57	10.2	3.3	0.56
100	TPU	20.1	3.7	0.69	6.7	3.0	0.66
	TPU-30	12.5	3.3	0.79	6.0	2.7	0.82
	TPU-75	15.2	3.4	0.62	6.6	3.0	0.60
	TPU-200	15.5	3.4	0.62	6.8	2.9	0.74
	TPU-650	14.5	3.4	0.68	7.7	2.9	0.74
800	TPU	9.6	3.3	0.67			
	TPU-30	10.2	3.3	0.69			
	TPU-75	11.0	3.3	0.59			
	TPU-200	11.2	3.3	0.55			
	TPU-650	10.9	3.4	0.54			
1200	TPU	11.5	3.2	0.58			
	TPU-30	10.6	3.2	0.82			
	TPU-75	11.8	3.2	0.66			
	TPU-200	9.7	3.2	0.72			
	TPU-650	10.3	3.2	0.67			

[a] Expected uncertainty due to sample variations and curve fitting.

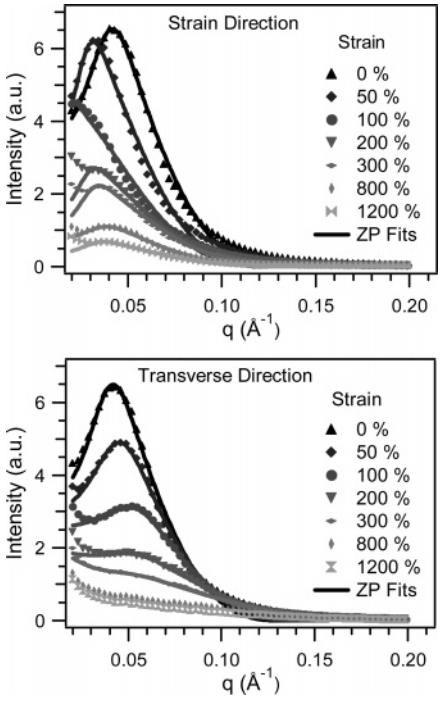

Figure 8. SAXS intensity of pure TPU averaged over 10° sectors and the associated Zernike−Prins fits in the (a) strain and (b) transverse directions.

and 1200%, where differences in the morphology of the TPU and nanocomposites may be expected on the basis of the tensile curves shown in Figure 4. The ZP model was able to reproduce the scattering peak and high q data over the entire strain range in the direction of strain. The ZP model was unable to fit the data in the transverse direction at high strains because the scattering peak had diminished, indicating that correlations between the hard segment structures had ceased to exist in the transverse direction.

1D SAXS profiles of the nanocomposites containing the smallest and largest silicates prior to silicate scattering subtraction are given in Figure 9. For comparison, SAXS profiles for the TPU host polymer at low (100%) and high (1200%) strain are also provided. These results suggest that the layered silicates do not have a significant effect on the TPU microphase morphology response to deformation, regardless of their size. Note that the small peak observed at $q = 0.2$ Å^{-1} for TPU-650 in the transverse direction is attributed to the basal spacing. Silicate scattering was subtracted in the same way as the unstrained samples, and the ZP fitting results obtained after the subtractions are tabulated in Table 3. The d and R values presented in Table 3 are similar for all of the materials, providing further evidence that the layered silicates did not have a significant effect on TPU microphase deformation.

The d values determined from the ZP fitting of the TPU host polymer are presented graphically in Figure 10. The solid lines in Figure 10 represent the expected d spacings for nondeformable domains undergoing affine deformation. The interdomain spacing is observed to increase in the strain direction up to 100% strain as deformation takes place predominately in the soft phase. Above 100% strain, d decreases in the strain direction, indicating that the domains are fragmenting into smaller structures. A decrease in d is observed at all strains in the transverse direction as expected for uniaxial flow. The R values presented in Table 3 are approximately the same in the strain and transverse directions prior to deformation.This indicates that the hard domains are either approximately spherical or randomly oriented and anisotropic. Laity et al.[26] observed an increase in R in the direction of strain and a decrease in R in the transverse direction, at low elongation. This behavior was attributed to the alignment of the long axis of anisotropic domains in the direction of strain, as opposed to hard domain elongation. This was a reasonable assumption given the higher modulus of the hard phase and because the features of the 2D scattering pattern at low strains can be reproduced by nondeformable spheres on a statistical lattice subjected to affine deformation.[23] In this study, R did not change significantly over the entire strain range, as might be expected during hard domain breakup. The data fitting was more sensitive to the position of the peak in the scattering profile, and hence the interdomain spacing (d), than to

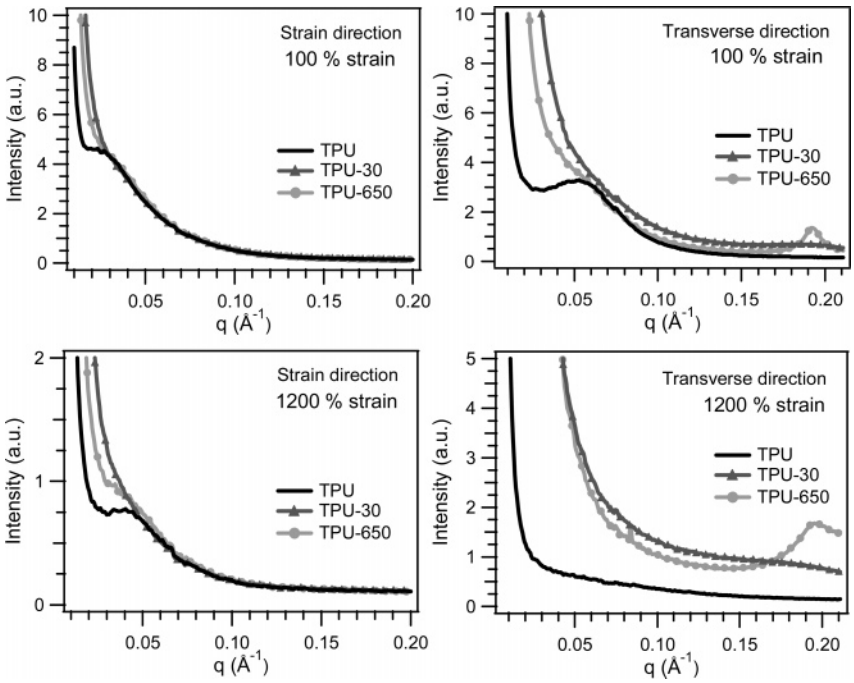

Figure 9. 1D SAXS profiles of TPU, TPU-30, and TPU-650 at low strain (100%) and high strain (1200%) prior to silicate scattering subtraction in the (a) strain and (b) transverse directions.

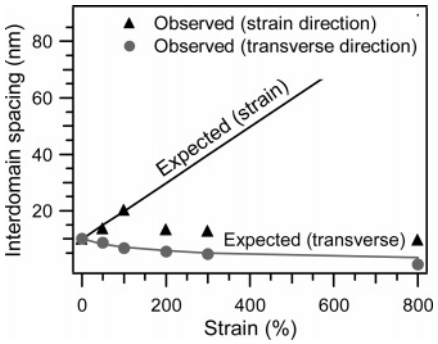

Figure 10. Average interdomain spacing of the pure TPU in the strain and transverse directions determined from the Zernike−Prins model. Solid lines represent expected values based on affine deformation.

the form factor contribution and hence the domain size (R).

While the ZP model does not provide insight as to whether the hard domains are approximately spherical or anisotropic, the small deviation between model and data at low elongation (50−100% strain) might indicate that the hard domains possess some degree of anisotropy. This is because the spherical domain assumption is only an approximation for randomly oriented anisotropic scattering bodies, and at low elongation anisotropic hard domains would be presumably aligned with their long axis in the direction of strain direction prior to their destruction.

Strain-Induced Soft Segment Crystallization. It was considered that the layered silicates may have an effect on the strain-induced crystallization of the soft segment and therefore the stress−strain properties of the TPU. The data collected in these experiments (data not shown) at the shortest camera length (0.1 Å^{-1} < q < 2.6 Å^{-1}) did not reveal any soft segment crystallization taking place during extension for any of the materials, thereby eliminating it as a possible cause for the observed tensile properties. Soft segment crystallization was observed by Yeh et al.[25] in a poly(urethane−urea) containing a PTMO soft segment of M_w = 1800 g/mol. In this study a PTMO of M_w = 1000 g/mol was utilized, which may have been sufficiently above its melting temperature to prevent strain-induced soft segment crystallization from taking place.

Discussion

The microphase morphology of TPUs has often been regarded as lamellar in the analysis of scattering data. Hard-sphere models have also been employed to analyze scattering data from various polyurethanes.[10,26,58−60] Most notably, hard-sphere models based on a Zernike-Prins type lattice and the Percus−Yevick liquid structure have been found to be consistent with the scattering from PTMO/MDI/BDO-based TPUs.[26,58] These models were found to accurately fit the scattering peak and high q data of the TPU studied here. This is not to say that the microdomains of this TPU should necessarily be considered as spherical. Laity[58] pointed out that these models may also be used to provide insight into the microstructure from TPUs that contain short, meandering, cylindrical or lamellar-type domains. The schematics shown in Figure 11 were developed in view of the composition and segment polydispersity of the TPU, the absence of any hard segment crystallization due to the solution casting and annealing process,[52] and the scattering analysis. These schematics were also influenced by Koberstein's partial miscibility model,[3,16] in which the longer hard segment sequences are forced to fold and reenter the domains, while shorter segments and single MDI units are soluble in the soft phase. This model illustrates that there is a significant proportion of hard segments present in the soft phase: a point often overlooked.

The schematic of the TPU-30 nanocomposite illustrates that even in the case of the smallest silicate studied here, the size scale of the microphase structure is still approximately one-third of the size of the filler particles and is an order of magnitude smaller than the larger particles. This is important to note because

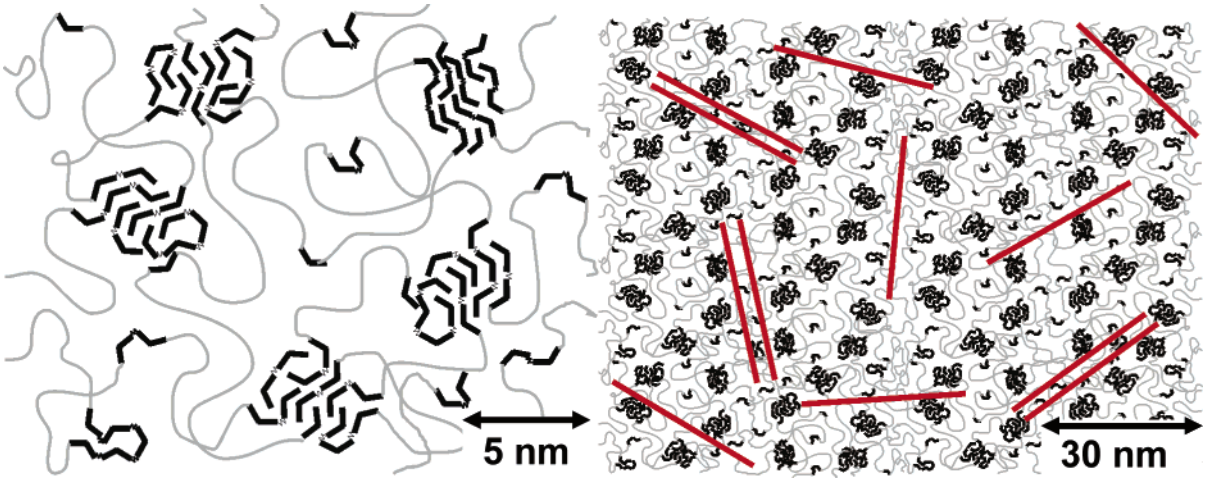

Figure 11. Phase morphology schematics of (a) TPU and (b) TPU-30 prior to deformation.

previously montmorillonite silicates approximately 100−200 nm in size have been represented on a length scale equivalent to that of the polyurethane microstructure.[72] Another important finding is that the hard microdomains are incapable of fitting in the interlayer spacing. This may indicate that the PTMO-rich phase occupies the interlayer spacing. While the SAXS and SANS results presented here have shown that the bulk TPU morphology is unchanged by the presence of these layered silicates, it is still expected that there may be differences at the polymer−filler interface and in the interlayer, which are not detected by these scattering techniques. As yet, we have been unable to obtain TEM images that are representative of the microstructure of this TPU, let alone visualize the TPU−filler interface. In future studies, these layered silicates will be incorporated into a recently synthesized polyurethane with monodisperse segments in which a globular-like domain morphology has been observed via TEM.[73]

In previous studies the ZP model had only been applied to the initial part of the stress−strain curve.[26] In this work the ZP model was used to fit the entire tensile curves of these materials. While the model adequately fit the high strain data in the strain direction, it should be mentioned that the spherical domain assumption becomes less valid at high strain where the scattering is expected to arise from correlations between elongated hard segment-rich structures, as opposed to hard domains. Nevertheless, the results obtained from the fitting combined with the direct visualization of the 1D scattering profiles have shown that the layered silicates did not have an observable effect on the morphological response of the TPU to deformation.

At high elongation the ability of the silicates to align in the direction of strain appears to be of great importance. In this study the smallest size fraction, MEE-30, was found to be more aligned than the larger silicates at high strain, presumably because of the lower spatial restrictions encountered in comparison to its larger counterparts. Large tactoids present in TPU-650, and to a lesser extent TPU-200, are less mobile and unable to align in the strain direction. Tactoids and unaligned platelets lead to tensile stresses between the polymer and filler resulting in void formation. Evidence for this is provided in the TEM image in Figure 12 from a nonmilled Somasif ME100 composite microtomed at the site of tensile failure. A void can be clearly observed at the site of the unaligned tactoid. More conclusive

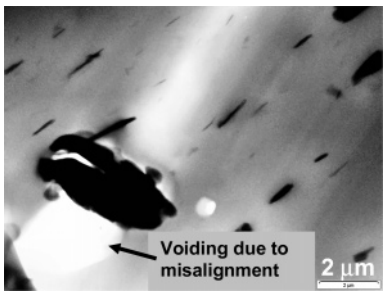

Figure 12. TEM image illustrating void formation at the site of an unaligned tactoid. Sample was microtomed at the site of tensile failure.

evidence for this mechanism was provided by the visualization of stress whitening in TPU-650, and to a lesser extent in TPU-200, which is indicative of void formation.[74] The pure TPU and the TPU-30 and TPU-75 nanocomposites remained relatively transparent throughout the tensile test. In the case of aligned silicates there are instead shear stresses as opposed to tensile stresses between the polymer and silicate, allowing for more effective stress transfer from the polymer to the filler.[55]

Also of importance is the interparticle distance at high strain. The silicates in TPU-30 and TPU-650 initially have an interparticle distance of ∼30 and ∼180 nm, respectively (Table 1). Assuming affine deformation, at 800% strain, the interparticle distance for MEE-30 would be expected to be 240 and 10 nm in the strain and transverse directions, respectively, while MEE-650 would have interparticle distances of 1600 and 60 nm in these directions, respectively. Clearly, a decrease in size leads to a reduction in interparticle distance and a significant increase in the amount of polymer influenced by the silicates at high strain. This is illustrated in the high strain schematics provided in Figure 13 (note the different scale bars employed). Therefore, as the size decreases, the stress transfer to the filler increases and polymer chain slippage is simultaneously reduced. While the polymer becomes more restrained with increasing diameter, the amount of polymer influenced by the silicates at high strain is insufficient to bring about the pronounced upturn in the tensile curve observed in TPU-30 and TPU-75. Also, as the size of the silicates increase, the presence of tactoids and voids acts to reduce the tensile properties, thereby countering any benefit possible from the larger fillers.

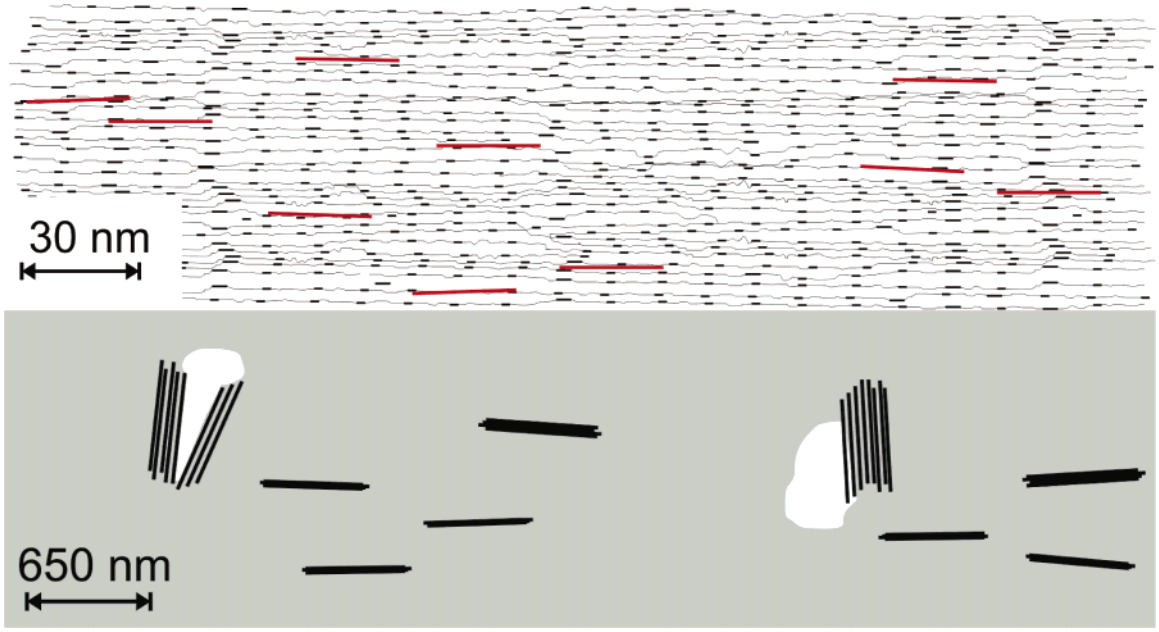

Figure 13. High-strain schematics of (a) TPU-30 and (b) TPU-650.

The interaction between the TPU and the filler is also a key factor in generating an upturn in the stress−strain curve. The dipolyoxyethylenemethylammonium surfactant allows for good silicate dispersion and hydrogen bonding to take place between the filler and the urethane-rich hard segment sequences and, to a lesser extent, the ether oxygens in the soft segment. It is believed that it is the hydrogen bonding between the polymer and filler that enables good stress transfer from the polymer to the filler and reduced chain slippage for strain hardening to occur. We have prepared composites containing silicates that are 30 nm in size with various surfactants, and only those that provide sufficient hydrogen bonding potential are able to promote an upturn in the stress−strain curve.

Summary

In summary, the findings of the SAXS/SANS studies are that the layered silicates do not have an observable effect on the microphase separation process during solution casting and annealing, nor do they affect the morphological response of the TPU to deformation, regardless of the platelet sizes studied here. In passing it would be quite desirable to investigate the effect of silicates that are smaller in size than the interdomain spacing (<10 nm) on the morphology and properties.

In terms of the stress−strain response it is proposed that the layered silicates have the following effects. At very low strains the layered silicates are able to increase the stiffness of the TPU through mechanical restrainment and hydrodynamic effects that increase with the diameter.[55,63,64] At intermediate strains the microphase structure dominates the properties, and the layered silicates have little influence on the stress−strain response. It is not until high elongation when the domain structure is disassembled and the silicates are well aligned that they are capable of interacting with the individual segments and imposing a significant influence on the tensile properties.

Acknowledgment. The authors thank Dr. Timothy Nicholson, Dr. Jeremy Ruggles, A/Prof Ian Gentle, and A/Prof Justin Cooper-White for useful discussions, Mr. Graham Ruhle for his contribution to the design of the tensometer, Dr. Philip Reynolds and Mr. Adam Perriman for assistance in running the SANS experiments, and Dr. Robert Knott for preliminary SANS data. Travel grants through the Australian Government Access to Major Facilities Program, the Royal Australian Chemical Institute Queensland Polymer Division Student Travel Program, and the University of Queensland Graduate School to access the scattering facilities are greatly acknowledged. This work was supported by a University of Queensland Postgraduate Research Scholarship. Use of the ChemMatCARS Sector 15 at the Advanced Photon Source was supported by the Australian Synchrotron Research Program, which is funded by the Commonwealth of Australia under the Major National Research Facilities Program. ChemMatCARS Sector 15 is principally supported by the National Science Foundation/Department of Energy under Grant CHE0087817 and by the Illinois Board of Higher Education. The Advanced Photon Source is supported by the US Department of Energy, Basic Energy Sciences, Office of Science, under Contract W-31-109-Eng-38.

References and Notes

(1) Bonart, R. *J. Macromol. Sci., Phys.* **1968**, *B2*, 115−138.
(2) Seymour, R. W.; Cooper, S. L. *Macromolecules* **1973**, *6*, 48−53.
(3) Koberstein, J. T.; Russell, T. P. *Macromolecules* **1986**, *19*, 714−720.
(4) Koberstein, J. T.; Galambos, A. F. *Macromolecules* **1992**, *25*, 5618−5624.
(5) Lee, H. S.; Yoo, S. R.; Seo, S. W. *J. Polym. Sci., Part B: Polym. Phys.* **1999**, *37*, 3233−3245.
(6) Saiani, A.; Rochas, C.; Eeckhaut, G.; Daunch, W. A.; Leenslag, J. W.; Higgins, J. S. *Macromolecules* **2004**, *37*, 1411−1421.
(7) Serrano, M.; Macknight, W. J.; Thomas, E. L.; Ottino, J. M. *Polymer* **1987**, *28*, 1667−1673.
(8) Tonelli, C.; Ajroldi, G.; Marigo, A.; Marega, C.; Turturro, A. *Polymer* **2001**, *42*, 9705−9711.
(9) Eisenbach, C. D.; Ribbe, A.; Gunter, C. *Macromol. Rapid Commun.* **1994**, *15*, 395−403.
(10) Chen-Tsai, C. H. Y.; Thomas, E. L.; Macknight, W. J.; Schneider, N. S. *Polymer* **1986**, *27*, 659−666.
(11) Li, C.; Cooper, S. L. *Polymer* **1990**, *31*, 3−7.

(12) Garrett, J. T.; Siedlecki, C. A.; Runt, J. *Macromolecules* **2001**, *34*, 7066−7070.
(13) McLean, R. S.; Sauer, B. B. *Macromolecules* **1997**, *30*, 8314−8317.
(14) O'Sickey, M. J.; Lawrey, B. D.; Wilkes, G. L. *J. Appl. Polym. Sci.* **2002**, *84*, 229−243.
(15) Aneja, A.; Wilkes, G. L. *Polymer* **2003**, *44*, 7221−7228.
(16) Koberstein, J. T.; Stein, R. S. *J. Polym. Sci., Part B: Polym. Phys.* **1983**, *21*, 1439−1472.
(17) Tyagi, D.; McGrath, J. E.; Wilkes, G. L. *Polym. Eng. Sci.* **1986**, *26*, 1371−1398.
(18) Koberstein, J. T.; Gancarz, I.; Clarke, T. C. *J. Polym. Sci., Part B: Polym. Phys.* **1986**, *24*, 2487−2498.
(19) Li, Y. J.; Gao, T.; Chu, B. *Macromolecules* **1992**, *25*, 1737−1742.
(20) Chu, B.; Gao, T.; Li, Y. J.; Wang, J.; Desper, C. R.; Byrne, C. A. *Macromolecules* **1992**, *25*, 5724−5729.
(21) Ryan, A. J.; Willkomm, W. R.; Bergstrom, T. B.; Macosko, C. W.; Koberstein, J. T.; Yu, C. C.; Russell, T. P. *Macromolecules* **1991**, *24*, 2883−2889.
(22) Bras, W.; Derbyshire, G. E.; Bogg, D.; Cooke, J.; Elwell, M. J.; Komanschek, B. U.; Naylor, S.; Ryan, A. J. *Science* **1995**, *267*, 996−999.
(23) Blundell, D. J.; Eeckhautb, G.; Fuller, W.; Mahendrasingam, A.; Martin, C. *Polymer* **2002**, *43*, 5197−5207.
(24) Desper, C. R.; Schneider, N. S.; Jasinski, J. P.; Lin, J. S. *Macromolecules* **1985**, *18*, 2755−2761.
(25) Yeh, F.; Hsiao, B. S.; Sauer, B. B.; Michel, S.; Siesler, H. W. *Macromolecules* **2003**, *36*, 1940−1954.
(26) Laity, P. R.; Taylor, J. E.; Wong, S. S.; Khunkamchoo, P.; Norris, K.; Cable, M.; Andrews, G. T.; Johnson, A. F.; Cameron, R. E. *Polymer* **2004**, *45*, 5215−5232.
(27) Stribeck, N.; Sapoundjieva, D.; Denchev, Z.; Apostolov, A. A.; Zachmann, H. G.; Stamm, M.; Fakirov, S. *Macromolecules* **1997**, *30*, 1329−1339.
(28) Fakirov, S.; Fakirov, C.; Fischer, E. W.; Stamm, M. *Polymer* **1991**, *32*, 1173−1180.
(29) Bonart, R.; Morbitzer, L.; Hentze, G. *J. Macromol. Sci., Phys.* **1969**, *B3*, 337−356.
(30) Khranovskii, V. A.; Gulko, L. P. *J. Macromol. Sci., Phys.* **1983**, *B22*, 497−508.
(31) Lilaonitkul, A.; Cooper, S. L. *Adv. Urethane Sci. Technol.* **1979**, *7*, 163−183.
(32) Reynolds, N.; Spiess, H. W.; Hayen, H.; Nefzger, H.; Eisenbach, C. D. *Macromol. Chem. Phys.* **1994**, *195*, 2855−2873.
(33) Seymour, R. W.; Allegrezza, A. E.; Cooper, S. L. *Macromolecules* **1973**, *6*, 896−902.
(34) Lin, S. B.; Hwang, K. S.; Tsay, S. Y.; Cooper, S. L. *Colloid Polym. Sci.* **1985**, *263*, 128−140.
(35) Estes, G. M.; Seymour, R. W.; Cooper, S. L. *Macromolecules* **1971**, *4*, 452−457.
(36) Ray, S. S.; Okamoto, M. *Prog. Polym. Sci.* **2003**, *28*, 1539−1641.
(37) Alexandre, M.; Dubois, P. *Mater. Sci. Eng.* **2000**, *28*, 1−63.
(38) Giannelis, E. P. *Adv. Mater.* **1996**, *8*, 29−35.
(39) Kojima, Y.; Usuki, A.; Kawasumi, M.; Okada, A.; Fukushima, Y.; Kurauchi, T.; Kamigaito, O. *J. Mater. Res.* **1993**, *8*, 1185−1189.
(40) Yurekli, K.; Karim, A.; Amis, E. J.; Krishnamoorti, R. *Macromolecules* **2003**, *36*, 7256−7267.
(41) Silva, A. S.; Mitchell, C. A.; Tse, M. F.; Wang, H. C.; Krishnamoorti, R. *J. Chem. Phys.* **2001**, *115*, 7166−7174.
(42) Krishnamoorti, R.; Silva, A. S.; Mitchell, C. A. *J. Chem. Phys.* **2001**, *115*, 7175−7181.
(43) Maiti, P.; Yamada, K.; Okamoto, M.; Ueda, K.; Okamoto, K. *Chem. Mater.* **2002**, *14*, 4654−4661.
(44) Wang, K. H.; Xu, M.; Choi, T. K.; Chung, I. J. *Polym. Bull. (Berlin)* **2001**, *46*, 499−505.
(45) Wang, K. H.; Choi, M. H.; Koo, C. M.; Xu, M. Z.; Chung, I. J.; Jang, M. C.; Choi, S. W.; Song, H. H. *J. Polym. Sci., Part B: Polym. Phys.* **2002**, *40*, 1454−1463.
(46) Balazs, A. C.; Singh, C.; Zhulina, E. *Macromolecules* **1998**, *31*, 8370−8381.
(47) Vaia, R. A.; Giannelis, E. P. *Macromolecules* **1997**, *30*, 7990−7999.
(48) Vaia, R. A.; Giannelis, E. P. *Macromolecules* **1997**, *30*, 8000−8009.
(49) Vaia, R. A.; Teukolsky, R. K.; Giannelis, E. P. *Chem. Mater.* **1994**, *6*, 1017−1022.
(50) Hasegawa, N.; Usuki, A. *Polym. Bull. (Berlin)* **2003**, *51*, 77−83.
(51) Gersappe, D. *Phys. Rev. Lett.* **2002**, *89*, 058301.
(52) Finnigan, B.; Martin, D.; Halley, P.; Truss, R.; Campbell, K. *Polymer* **2004**, *37*, 2149−2160.
(53) Yang, J. H.; Han, Y. S.; Choy, J. H.; Tateyama, H. *J. Mater. Chem.* **2001**, *11*, 1305−1312.
(54) Campbell, K. PhD Thesis, School of Engineering, The University of Queensland, Brisbane, 2005.
(55) Fornes, T. D.; Paul, D. R. *Polymer* **2003**, *44*, 4993−5013.
(56) Wignall, G. D.; Bates, F. S. *J. Appl. Crystallogr.* **1987**, *20*, 28−40.
(57) Koberstein, J. T.; Stein, R. S. *J. Polym. Sci., Part B: Polym. Phys.* **1983**, *21*, 2181−2200.
(58) Laity, P. R.; Taylor, J. E.; Wong, S. S.; Khunkamchoo, P.; Norris, K.; Cable, M.; Andrews, G. T.; Johnson, A. F.; Cameron, R. E. *Polymer* **2004**, *45*, 7273−7291.
(59) Visser, S. A.; Pruckmayr, G.; Cooper, S. L. *Macromolecules* **1991**, *24*, 4, 6769−6775.
(60) Krakovsky, I.; Bubenikova, Z.; Urakawa, H.; Kajiwara, K. *Polymer* **1997**, *38*, 3637−3643.
(61) King, S. M. In *Modern Techniques for Polymer Characterisation*; Pethrick, R. A., Dawkins, J. V., Eds.; John Wiley & Sons: New York, 1999; Chapter 7.
(62) Kim, G. M.; Lee, D. H.; Hoffmann, B.; Kressler, J.; Stoppelmann, G. *Polymer* **2001**, *42*, 1095−1100.
(63) Masenelli-Varlot, K.; Reynaud, E.; Vigier, G.; Varlet, J. *J. Polym. Sci., Part B: Polym. Phys.* **2002**, *40*, 272−283.
(64) Brune, D. A.; Bicerano, J. *Polymer* **2002**, *43*, 369−387.
(65) Roe, R. J. *Methods of X-ray and Neutron Scattering in Polymer Science*; Oxford University Press: New York, 2000.
(66) Malwitz, M. M.; Lin-Gibson, S.; Hobbie, E. K.; Butler, P. D.; Schmidt, G. *J. Polym. Sci., Part B: Polym. Phys.* **2003**, *41*, 3237−3248.
(67) Vaia, R. A.; Liu, W. D.; Koerner, H. *J. Polym. Sci., Part B: Polym. Phys.* **2003**, *41*, 3214−3236.
(68) Tateyama, H.; Noma, H.; Nishimura, S.; Adachi, Y.; Ooi, M.; Urabe, K. *Clays Clay Mineral.* **1998**, *46*, 245−255.
(69) Breu, J.; Seidl, W.; Stoll, A. J.; Lange, K. G.; Probst, T. U. *Chem. Mater.* **2001**, *13*, 4213−4220.
(70) Klapyta, Z.; Gawel, A.; Fujita, T.; Iyi, N. *Clay Mineral.* **2003**, *38*, 151−160.
(71) Pedersen, J. S. *J. Appl. Crystallogr.* **1994**, *27*, 595−608.
(72) Tien, Y. I.; Wei, K. H. *Polymer* **2001**, *42*, 3213−3221.
(73) Unpublished work.
(74) Nathani, H.; Dasari, A.; Misra, R. D. K. *Acta Mater.* **2004**, *52*, 3217−3227.

MA0508911